Check for updates

Optical oxygen saturation imaging in cellular ex vivo lung perfusion to assess lobular pulmonary function

DAISUKE SAKOTA,[1,*] ⓘ RYO KOSAKA,[1] HIROMICHI NIIKAWA,[2] KATSUHIRO OHUCHI,[3] HIROKUNI ARAI,[4] KENNETH R. MCCURRY,[5,6,7] AND TOSHIHIRO OKAMOTO[5,6,7,8]

[1] *Health and Medical Research Institute, National Institute of Advanced Industrial Science and Technology (AIST), Tsukuba, Ibaraki 3058564, Japan*
[2] *Department of Thoracic Surgery, Institute of Development, Aging and Cancer, Tohoku University, Sendai, Miyagi 9808575, Japan*
[3] *Department of Advanced Surgical Technology Research and Development, Graduate School of Medical and Dental Sciences, Tokyo Medical and Dental University, Tokyo 1138519, Japan*
[4] *Department of Cardiovascular Surgery, Graduate School of Medical and Dental Sciences, Tokyo Medical and Dental University, Tokyo 1138519, Japan*
[5] *Department of Thoracic and Cardiovascular Surgery, Cleveland Clinic, Cleveland, OH 44195, USA*
[6] *Department of Inflammation and Immunology, Lerner Research Institute, Cleveland Clinic, Cleveland, OH 44195, USA*
[7] *Transplant Center, Cleveland Clinic, Cleveland OH 44195, USA*
[8] *okamotto@ccf.org*
[*] *sakota.ao@aist.go.jp*

Abstract: Ex vivo lung perfusion (EVLP) is an emerging tool to evaluate marginal lungs in lung transplantation. However, there is no objective metric to monitor lobular regional oxygenation during EVLP. In this study, we developed oxygen saturation (SaO_2) imaging to quantitatively assess the regional gas exchange potential of the lower lobes. Ten porcine lungs were randomly divided into control and donation after circulatory death (DCD) groups (n = 5, each). Lungs were perfused in cellular EVLP for 2 h, and multispectral images were continuously collected from the dorsal sides of the lower lobes. We examined whether lower lobe SaO_2 correlated with PaO_2/FiO_2 (P/F) ratios in lower pulmonary veins (PV). The wet/dry ratio in lower lobes was measured and Monte Carlo simulations were performed to investigate the method's feasibility. There was a significant correlation between lower lobe SaO_2 and the P/F ratio in lower PV (r = 0.855, $P < 0.001$). The DCD group was associated with lower SaO_2 and higher wet/dry ratio than the control group ($P < 0.001$). The error of estimated SaO_2 was limited according to Monte Carlo simulations. The developed technology provides a noninvasive and regional evaluative tool of quantitative lobular function in EVLP.

1. Introduction

Ex vivo lung perfusion (EVLP) has been utilized to expand the donor lung pool in clinical lung transplantation using marginal criteria donors. In Lund-type EVLP, the perfusate containing red blood cells (RBCs) ensures high reliability of blood gas analysis for transplant suitability [1]. The PaO_2/FiO_2 (P/F) ratio is a key criterion in the evaluation, with a threshold of 300 mmHg [2,3]. Although blood gas analysis from the left atrium (LA) is useful for the global assessment of double lungs, differential blood gas analysis from each pulmonary vein (PV), palpation, deflation test, and bronchoscopy are important tools in the assessment of regional and lobular lung function. Costa et al. reported that differential blood gas analysis provides a more accurate assessment of regional lung function than blood gas analysis in LA in clinical

donor procurement [4]. Moreover, Freitag et al. developed a novel bronchoscopic method for gas exchange assessment of lobes and lung segments [5]. Both approaches, however, allow only intermittent evaluation, and the bronchoscopy technique is invasive and might interfere with the EVLP protocol, including deflation of the lungs. Currently, there is no continuous and noninvasive imaging technology to evaluate regional oxygenation in EVLP.

Hyperspectral and multispectral imaging (MSI) is a method providing spectrally resolved information at each pixel of an acquired image. MSI can be achieved by combining a camera and many different spectroscopic technologies such as multi-position filter-wheels, gratings and prisms, laser-scanning single point spectrographs, electronically adjustable tunable filters, and Fourier-transform imaging spectroscopy [6]. MSI was first developed for remote sensing in planetary science and astronomy [7]. In general, biological tissue is optically turbid media. The optical properties of biological tissue, which are light scattering and absorption coefficient, are affected by the pathological condition and biological activity. Therefore, MSI has been rapidly developed for medical applications, offering great potential for a technique of quantitative diagnosis [8]. Especially, the use of MSI in oxygen saturation (SaO_2) imaging has been focused on for the diagnosis of retina hypoxia and skin mottling [9,10]. Visible and near-infrared wavelengths, which range from 650 to 1000 nm, are easy-to-use, penetrate into tissue, and the light absorption sensitivity is altered by oxy- and deoxy-hemoglobin in blood flow. Moreover, for organ perfusion, Tetschke et al. demonstrated that MSI discriminates between perfused and non-perfused areas when monitoring SaO_2 during kidney perfusion [11]. The application of MSI to lung perfusion, however, has not yet been reported.

Basically, optical SaO_2 imaging depends on the difference in light absorption at two or more wavelengths [12,34]. The difference in light absorption is determined by the optical path length through the scattering in biological tissue. Therefore, the optical properties of the tissue are important for accurate quantitative diagnosis by MSI. Beak et al. investigated optical properties of non-perfused explanted piglet lung in different ventilation status at 632.8 nm [13]. Yi et al. measured the optical properties of deflated rat lung by inverse spectroscopic optical coherence tomography at 630 nm [14]. Jacques modeled the relationship between optical properties of various biological tissue including lung and wavelengths [15]. We hypothesized that SaO_2 imaging will reflect regional oxygenation of the lower lobes in cellular EVLP. Here, we developed a novel quantitative, real-time, and noninvasive method to image SaO_2 by MSI using visible and near-infrared light in a porcine lung EVLP model. The accuracy of SaO_2 imaging was analyzed using Monte Carlo simulation in the reported range of optical properties in lung.

2. Methods

2.1. Study design

Ten pigs were randomly divided into a control group and donation after circulatory death (DCD) group (n = 5, each). In the control group, lungs were perfused in EVLP following 1 h of cold ischemic time. In the DCD group, lungs were perfused after 90 min of warm ischemic time and a subsequent 5 h of cold ischemic time. During EVLP, MSI images of the dorsal sides in the lower lobes were continuously recorded. The following parameters were collected at 1 and 2 h: P/F ratio in LA, P/F in lower PV, and airway parameters. At 2 h, lung tissues were obtained to calculate wet/dry (W/D) ratios and lung weight gain.

2.2. Animal preparation

Males, crossbred between Landrace and Large White pigs (42-49 kg), were used. Tracheal intubation followed subcutaneous injection of 2 mg/kg xylazine and 20 mg/kg ketamine, and isoflurane of 1.5-3.0% was started. In the control group, lungs were procured in a standard fashion [16]. Two liters of Perfadex + nitroglycerin 10 mg/L was flushed antegrade in the pulmonary

artery (PA), and 1 L of Perfadex was used for cold storage. In the DCD group, 500 units/kg heparin was intravenously administered, and after 3 min, pigs were sacrificed by intravenous injections of potassium chloride (2.0 mEq/kg). Following cardiac arrest, the pigs were kept in a supine position for 90 min, and lungs were procured in the same manner as in the control group. Blood was collected from a blood donor pig, and packed RBCs were prepared by a cell saver (XTRA; LivaNova Japan K. K., Tokyo, Japan). This study was approved by the Institutional Animal Care and Use Committees of the National Institute of Advanced Industrial Science and Technology (Approval number #2020-0336) and Tokyo Medical and Dental University (Approval number #A2020-100C). All methods were carried out in accordance with relevant guidelines and regulations.

2.3. Cellular EVLP

The organ chamber was made of optically transparent polycarbonate to capture MSI (Fig. 1(A)). All optical instruments, including a light source, mirror, and hyperspectral camera (HSi-300; Gooch&Housego Inc., Ilminster, UK), were compacted under the chamber so as not to interfere with EVLP operation. Lungs were perfused according to the Lund protocol as previously reported [17–19]. Briefly, the system was primed with 2.0 L of STEEN solution, heparin 10,000 IU, imipenem 100 mg, and 500 mL of packed RBCs. Hematocrit (Ht) levels in the perfusate were maintained in a range of 10-15%. During the recondition phase, a gas mixture of O_2, N_2, and CO_2 was delivered to the membrane at flow rates of 2.7, 9.3, and 0.7 L/min, respectively. LA was left open. The flow rate increased in a stepwise fashion to a target flow of 70 mL/kg/min. Lungs were ventilated with the following settings when the lung temperature reached 36°C: Tidal volume (TV) 6 mL/kg, respiratory rate (RR) 7 breaths/min, positive end-expiratory pressure (PEEP) 5 cm H_2O, and FiO_2 0.4. At 50 min, the following recruitment maneuver was performed: TV 10 mL/kg, RR 10 breaths/min, PEEP 5 cm H_2O, and FiO_2 0.4 for 10 min. Then the O_2 gas supply to the membrane was stopped.

2.4. Blood gas analysis

For LA blood gas analysis, 2.5 mL of perfusate from each PV was collected in a small cup (10 mL) and mixed before being measured. For differential blood gas analysis of lower lobes, 2.5 mL of perfusate was obtained through a baby catheter located in each lower PV (outer diameter, 1.8 mm). PaO_2 and SaO_2 in the LA and lower PV at FiO_2 of 0.4, 1.0, and 0.21 were measured at 1 and 2 h by using a blood gas analyzer (ABL80 FLEX; Radiometer KK, Tokyo, Japan).

2.5. SaO_2 image processing from MSI

A xenon light source (MAX303; Asahi Spectra Co., Ltd., Tokyo, Japan) was used, and the light was guided by an optical fiber. A rod lens (RLQL80-2; Asahi Spectra Co., Ltd.) was attached to the outlet port of the fiber to uniformly illuminate the dorsal side of the lungs. The backscattering light was continuously captured throughout EVLP via a mirror by an acoustic-optic tunable filter (AOTF)-based hyperspectral camera with a capture time of 400 ms/image at the resolution of 0.3 mm/pixel ($10^3 \times 10^3$ pixels) and the out-of-band rejection of -30 dB. A normal RGB image taken by a digital video camera (HDR-CX120; Sony Corp., Tokyo, Japan) is shown in Fig. 1(B). The MSI was created from 12 sub-images of each wavelength (Range: 590-913 nm, Fig. 1(C)). To create an SaO_2 image, two images at 650 and 800 nm were extracted from the MSI (Fig. 1(D)). In this study, we employed the simplest method proposed by Polanyi et al. [12]. The relationship between SaO_2 and the backscattering intensity of the two lights from the tissue was formulated as follows:

$$\Delta R(x, y) = I_{650nm}(x, y)/I_{800nm}(x, y) = \alpha \times SaO_2(x, y) + \beta \tag{1}$$

where $\Delta R(x,y)$ is the proportion value of two wavelengths at coordinates of x and y of the image, and $I_{650nm}(x,y)$ and $I_{800nm}(x,y)$ are brightness values at wavelengths of 650 nm and 800 nm.
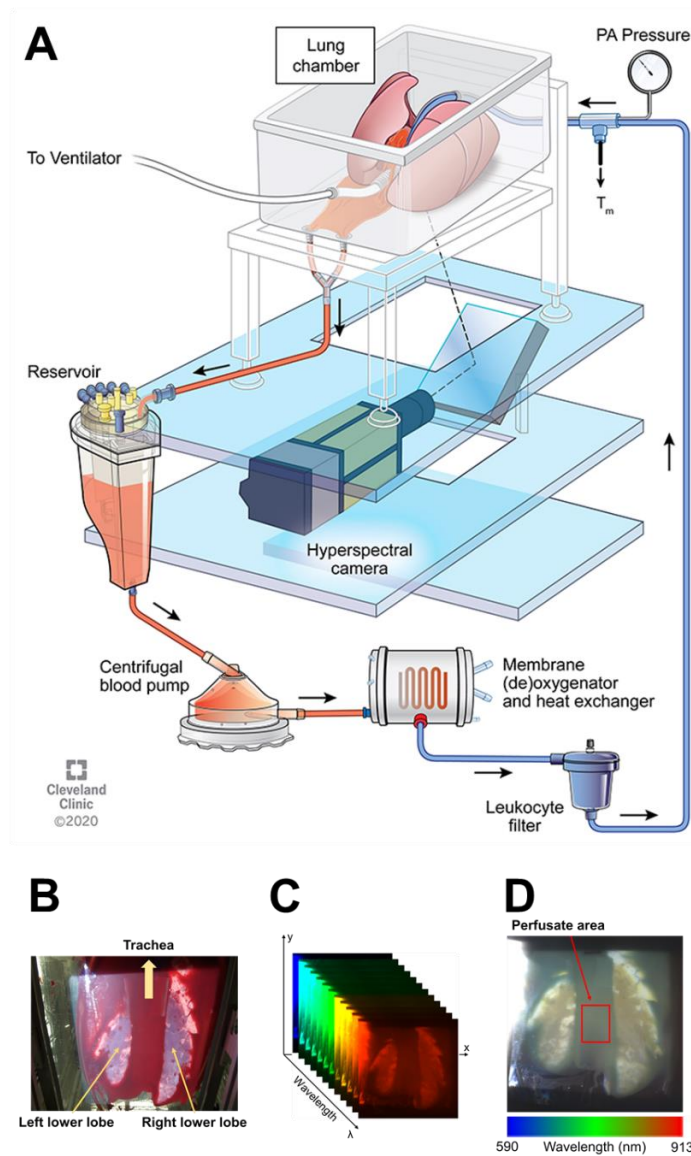
Fig. 1. (A) Developed EVLP with optical imaging system. A hyperspectral camera collected light from the dorsal side of lungs via an optically transparent chamber and a mirror. (B) RGB image of the dorsal sides of lungs (e.g. the DCD group). Perfusate flowed out from LA and then stayed between right and left lungs for a while before moving to the reservoir. (C) Creation of multispectral image (MSI). The MSI was created by layering the 12 sub-images of each wavelength in the range from 590 to 913 nm (590, 620, 650, 680, 710, 740, 770, 800, 830, 860, 890, 913 nm) and coloring them. The bandwidth was 16.8 nm. (D) MSI of dorsal side of lungs (e.g. the DCD group). Red-rectangular indicates the area where two sub-images at 650 nm and 800 nm were extracted for ΔR calculation. This area corresponds to the outflow of LA.

The light absorption at 650 nm significantly depended on SaO_2, while that at 800 nm was an isosbestic wavelength and did not depend on SaO_2. The constant values of α and β depended on

the light intensity, detection sensitivity, and optical properties of the lungs. The SaO_2 data of blood gas analysis from LA at 1 and 2 h were compared to ΔR in the LA outflow area where the perfusate flowed out (Fig. 1(D)). There was a significant correlation between SaO_2 and ΔR (n = 60, r = 0.881, ΔR = 0.033 × SaO_2 -1.621, Fig. 2).
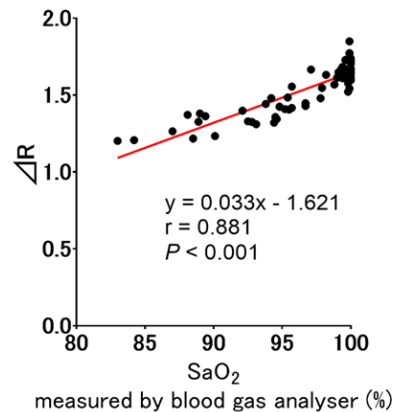

Fig. 2. Relationship between ΔR and SaO_2 of perfusate from the left atrium. n = 60; 10 cases (Control, n = 5; DCD, n = 5), two evaluation times (1 and 2 h), three FiO_2.

2.6. Correlation between lower lobe SaO₂ estimated by MSI and P/F ratio in lower PV

Typical MSI images and corresponding SaO_2 imaging at an FiO_2 of 1.0 are shown in Fig. 3(A). The SaO_2 was calculated according to the formula of the correlation between ΔR and SaO_2 (Fig. 2). The areas circled by solid lines indicate the lower lobes. The areas outside the solid lines reflect oxygenated perfusate coming from LA outflow. The histogram of lower lobe SaO_2 is shown in Fig. 3(B). In addition to a single peak at 100%, there was an isolated peak at 98% in the control group, whereas there were two peaks at 86% and 97% in the DCD group. Lower lobe SaO_2 calculated by MSI ($SaO_{2\ MSI}$) was defined as the median point in the histogram of each lower lobe. Then, lower lobe $SaO_{2\ MSI}$ were compared with corresponding P/F ratios in the lower PV.

2.7. Relationship between lower lobe SaO₂ MSI and W/D ratio

To collect lung tissue samples for W/D ratio assessment from the location corresponding to SaO_2 imaging, the lower lobe dorsal surface (white dotted line area, Fig. 4(A)) was equally divided into three areas: top, middle, and bottom. Then, each area was further divided into four equal subareas according to the gravity point of each area. Lung samples (Size; 1 × 1 × 1 cm, n = 6, each side) were obtained (Fig. 4(A)). In parallel, SaO_2 data (FiO_2 = 1.0) at 2 h were collected from the area (Size: 1 × 2.5 cm) covering the corresponding two lung tissue sampling locations in each area (Fig. 4(B)). The correlation between mean W/D value of two subareas and SaO_2 data in each area was analyzed. Lung tissue was frozen at -80°C and dried at 60°C for 24 h for W/D ratio calculation.

2.8. Monte Carlo simulations of light propagation in lungs

To verify the validity of SaO_2 imaging in lung tissue, Monte Carlo simulations were conducted. The simulation program proposed by Wang was used [20]. According to Jacques [15], the
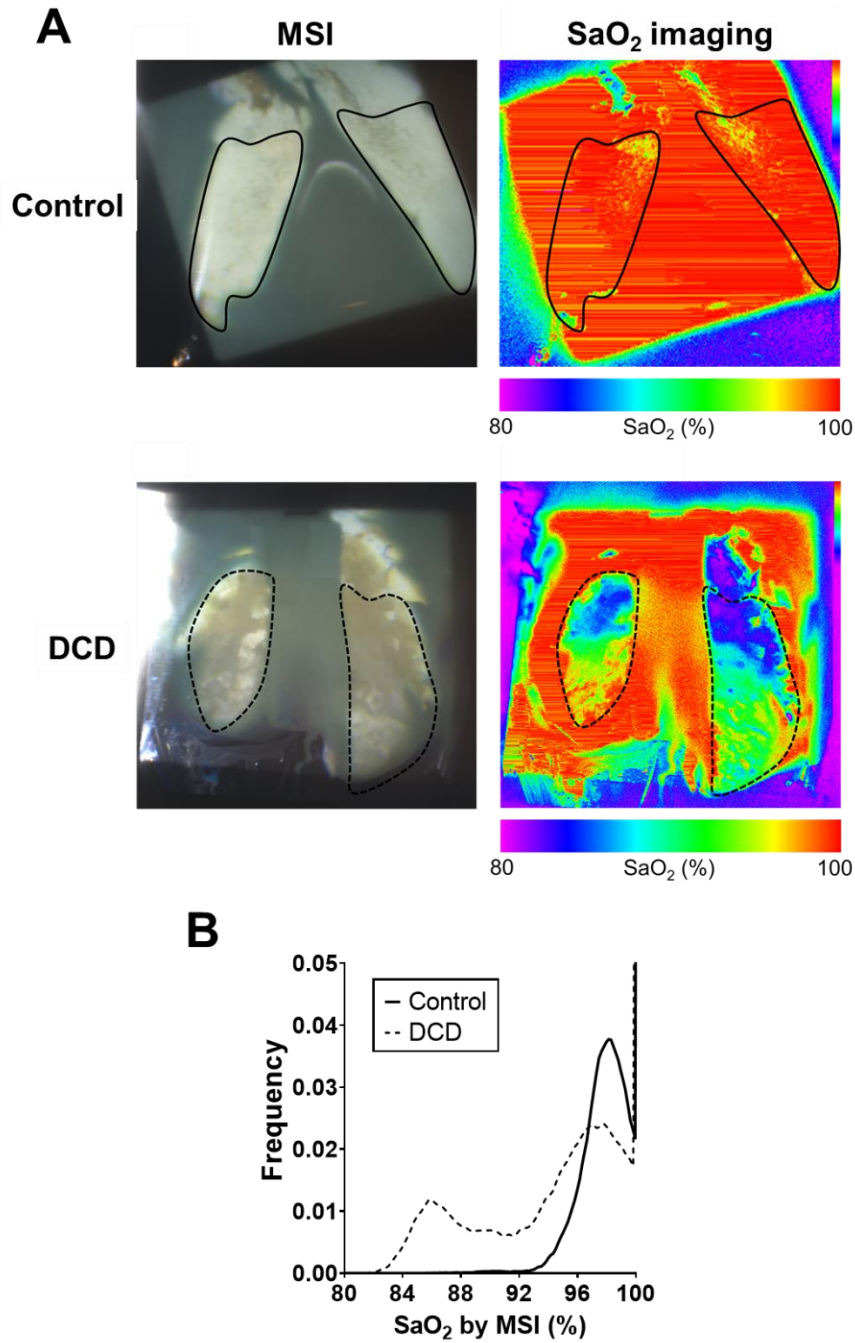
Fig. 3. (A) Typical finding of MSI and SaO_2 imaging in the control and DCD groups ($FiO_2 = 1.0$). (B) SaO_2 histogram of a lower lobe of the case shown in Fig. 3(A). The data was obtained within the solid or dotted line of the lower lobe. Lower lobe $SaO_{2\ MSI}$ was defined as the median point of the histogram.

reduced scattering coefficient of tissues was estimated by the following equation:

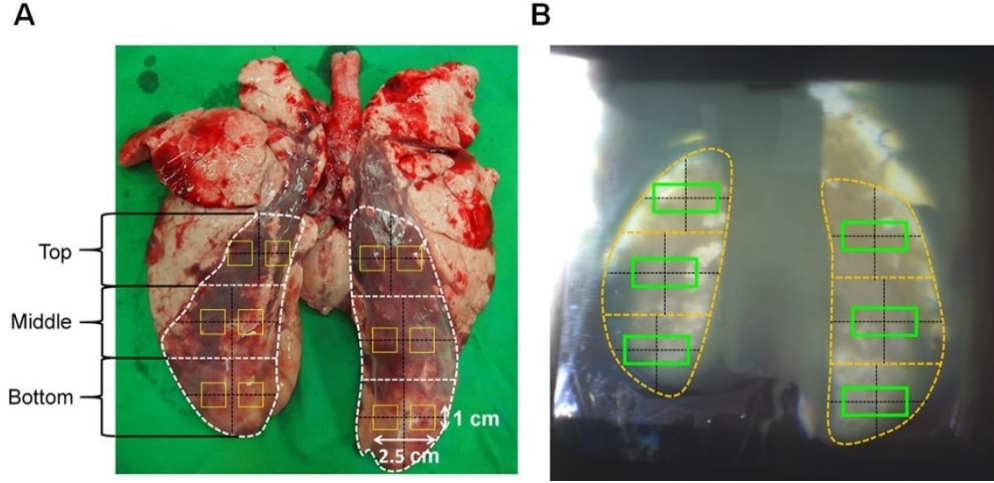$$\mu_s' = a\left(\frac{\lambda}{500(nm)}\right)^{-b} \tag{2}$$

Fig. 4. (A) Lung tissue sampling for W/D ratios at the end of EVLP. Lower lobes were equally divided into three areas: top, middle, and bottom. Then, lung tissues at the two yellow-marked squares were collected in each area. (B) SaO$_2$ image collection in the evaluation phase at 2 h (FiO$_2$ = 1.0). SaO$_2$ images in each green-marked rectangle were collected in each area.

where $\mu_s = \mu_s(1 - g)$; μ_s is the scattering coefficient (cm^{-1}) and g is the anisotropy factor. In this study, the g of lungs was 0.95 as a typical value [14,15]. In the equation, the wavelength λ is normalized by a reference wavelength, 500 nm, to yield a dimensionless value, which is then raised to the power b, called the 'scattering power'. This term characterizes the wavelength dependence of μ_s' which is the reduced scattering coefficient (cm^{-1}). The factor a is the value μ_s' (λ = 500 nm), which scales the wavelength-dependent term. However, the μ_s' of the lung varies in the literature. The ranges of a and b were 8.1-25.4 and 0.53-0.98, respectively [14, 15,21]. Then, μ_s' (λ = 650 nm) and μ_s' (λ = 800 nm) varied from 6 to 22 cm^{-1} and 5 to 20 cm^{-1}, respectively. Therefore, in this study, we performed Monte Carlo simulations by using the entire range of reported μ_s' values of the lungs to investigate the possible errors in SaO$_2$ estimation depending on the optical properties of the lung tissue. Here, we considered that the reduced scattering coefficient of the lung, $\mu_{s\,Lung}'$ can be described by a synthetic reduced scattering coefficient of perfusate ($\mu_{s\,Perfusate}'$) and skeleton ($\mu_{s\,Skeleton}'$). Skeleton is defined as a component of lung parenchyma without pulmonary intravascular perfusate. The formula is as follows:

$$\mu_{s\,Lung}' = k \times \mu_{s\,Perfusate}' + (1 - k) \times \mu_{s\,Skeleton}' \tag{3}$$

$$\mu_{a\,Lung} = k \times \mu_{a\,Perfusate} \tag{4}$$

where k (0 ≤ k ≤ 1) is the mixing ratio of perfusate and skeleton. Then the scattering and absorption coefficients of perfusate were calculated by the following equations [22,25]:

$$\mu_{s\,Perfusate} = \frac{Ht(1 - Ht)}{V}\sigma_s \tag{5}$$

$$\mu_{a\,Perfusate} = 2.303 \times e(\lambda) \times \frac{10 \times tHb}{mHb} \tag{6}$$

where Ht is the hematocrit (0 ≤ Ht ≤ 1), V is the mean corpuscular volume, and σ_s is the scattering cross-section of RBC. In this study, a value of 50 μm^3 was used for V as reported in porcine RBC [22,23]. The value of 44 μm^2 for μ_s' (λ = 800 nm) is derived from Mie theory [24], where
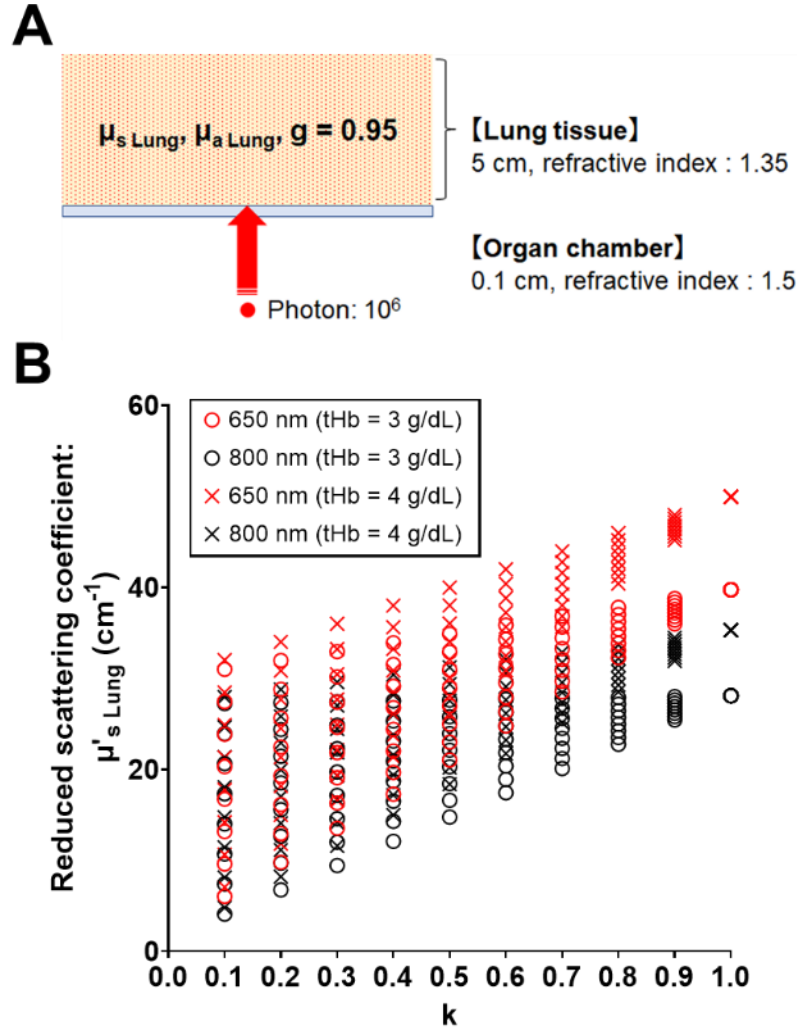
Fig. 5. (A) Monte Carlo simulation model of the lung. Photons (10^6) irradiated the lung tissue, which was located in the organ chamber. The thickness and the refractive index of the organ chamber were 0.1 cm and 1.5, respectively. The thickness and the refractive index of the lung were 5 cm and 1.35, respectively. The simulation outputted the defuse reflectance to calculate ΔR and Eq. 8). (B) Reduced scattering coefficient of lung, $\mu'_{s\ Lung}$. At 650 nm, $\mu'_{s\ Lung}$ at (Ht = 0.10, tHb = 3 g/dL) was 6-40 cm^{-1}, and $\mu'_{s\ Lung}$ at (Ht = 0.13, tHb = 4 g/dL) was 7-50 cm^{-1}. At 800 nm, $\mu'_{s\ Lung}$ at (Ht = 0.10, tHb = 3 g/dL) was 4-28 cm^{-1}, and $\mu'_{s\ Lung}$ at (Ht = 0.13, tHb = 4 g/dL) was 5-35 cm^{-1}.

the relative refractive index between RBC and extracellular fluid was 1.04 and the anisotropy factor of RBC was g = 0.99 [22]. Equation (6) was proposed by Prahl [25], and e(λ) is the molecular extinction coefficient for the wavelength λ in cm^{-1}/mol/l. mHb is the molecular weight of hemoglobin (64,500 g/mol). tHb is the total hemoglobin of perfusate in g/dL. In this study, the mean ± standard deviation of Ht and tHb were 0.127 ± 0.09 and 3.9 ± 0.9 g/dL, respectively. Then, in the simulation, the two pairs of (Ht = 0.1, tHb = 3 g/dL) and (Ht = 0.13, tHb = 4 g/dL) were used in Eq. (5) and Eq. (6), respectively. Furthermore, e(λ) is dependent on SaO$_2$ as follows:

$$e(\lambda) = SaO_{2\ Perfusate} \times e_{HbO_2}(\lambda) + (1 - SaO_{2\ Perfusate}) \times e_{Hb}(\lambda) \tag{7}$$

where, $e_{HbO_2}(\lambda)$ and $e_{Hb}(\lambda)$ are the molecular extinction coefficients of oxy- and deoxy-hemoglobin, respectively. In Monte Carlo simulations, the following values were used: $e_{HbO_2}(650\ nm) = 368$ cm^{-1}/mol/l, $e_{Hb}(650\ nm) = 3750$ cm^{-1}/mol/l, $e_{HbO_2}(800\ nm) = 816$ cm^{-1}/mol/l, $e_{Hb}(800\ nm) = 762$ cm^{-1}/mol/l. The SaO$_{2\ Perfusate}$ $(0 \leq SaO_{2\ Perfusate} \leq 1)$ is the oxygen saturation in the lung, where SaO$_{2\ Perfusate}$ is considered as the SaO$_2$ of the mixed blood of PA and PV. In the simulation, three values of 0.8, 0.9, and 1.0 for SaO$_{2\ Perfusate}$ were used. The simulation model is shown in Fig. 5(A). The number of photons was 10^6. $\mu'_{s\ Lung}$ in Eq. (3) is shown in Fig. 5(B). Since $\mu'_{s\ Perfusate}$ was larger than $\mu'_{s\ Skeleton}$, $\mu'_{s\ Lung}$ decreased as k decreased. In addition, $\mu'_{s\ Lung}$ fluctuated because $\mu'_{s\ Skeleton}$ varied from 2 to 30 cm^{-1} at 650 nm and from 1 to 27 cm^{-1} at 800 nm. The value becomes higher as the tHb increases.

ΔR in the simulation was calculated by dividing the diffuse reflectance intensity at 650 nm by the one at 800 nm. The SaO$_2$ in the lung was finally calculated by the following equation:

$$SaO_{2\ Lung} = \frac{\Delta R}{\Delta R_{k=1}} \times SaO_{2\ Perfusate} \tag{8}$$

where $\Delta R_{k=1}$ means the ΔR in perfusate simulated at k = 1.

2.9. Statistical analysis

Statistical analysis was performed using JMP version 15.2.1 (SAS Institute Inc., Cary, NC, USA). Data are expressed as a median and a range (minimum-maximum). Correlations between two sets of parametric data was analyzed by Pearson's correlation coefficient. Student's *t* test was used for parametric data. The breakpoint of the P/F ratio vs. lower lobe SaO$_2$ was identified by piecewise linear function fitting. A value of *P* < 0.05 was considered statistically significant.

3. Results

3.1. EVLP parameters

All 10 cases were completed at the target final flow rate of 3.0 (3.0-3.2) L/min. At 2 h, the DCD group was significantly associated with a lower P/F ratio in LA (FiO$_2$ = 1.0, 274 [155 - 422] vs. 461 [414 - 454] mmHg, *P* = 0.008), higher peak inspiratory pressure (15 [11–17] vs. 10 [9.5 - 10] cmH$_2$O, *P* = 0.001), and lung weight gain (+303 [+194 to +534] vs. -11[-36 to +8] g, *P* = 0.002), compared with the control group.

3.2. Trend of SaO$_2$ imaging

The typical trend of SaO$_2$ images at 1 h is shown in Fig. 6. In the recondition phase, where the PO$_2$ of PA was 229 (188-348) mmHg, most of the area in both groups was red, corresponding to a SaO$_2$ of 100%. Following the shutoff of O$_2$ gas supply to the membrane, the color in the control group was consistently red, except the green part in the top area at an FiO$_2$ of 0.21. In contrast, the color in the DCD group changed depending on the three FiO$_2$. The top area tended to be blue, while the middle and bottom areas were either green or red.
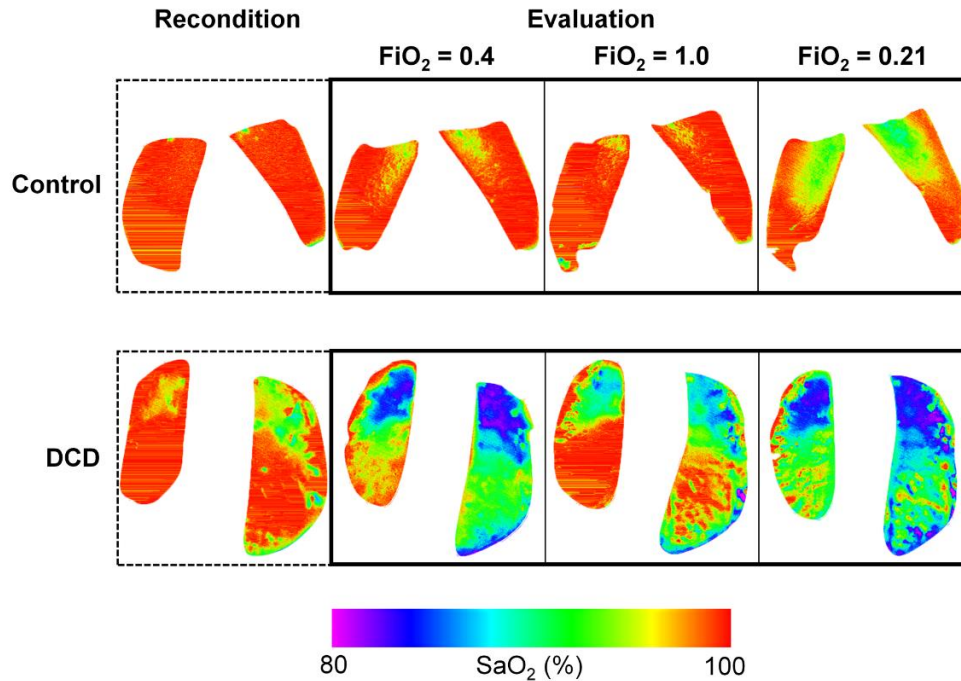
Fig. 6. Typical SaO_2 image changes during recondition and evaluation phases at 1 h in the control and the groups. Red and purple colors correspond to 100% and 80% of SaO_2, respectively.

3.3.   *Significant correlation between lower lobe $SaO_{2\ MSI}$ and P/F ratio in lower PV*

There was a significant correlation between lower lobe $SaO_{2\ MSI}$ and P/F ratios in the lower PV (FiO_2 = 0.4, 1.0, or 0.21, n = 120, r = 0.591, $P < 0.001$, Fig. 7(A)). Next, subgroup analysis was performed for each FiO_2. After having identified a breakpoint, a linear correlation was analyzed by using a value below the plateau. The maximum linear correlation was observed for an FiO_2 of 1.0 (Fig. 7(B)–7(D)).

3.4.   *Significant differences in $SaO_{2\ MSI}$ and W/D ratios of three areas in the lower lobes*

The top, middle, and bottom $SaO_{2\ MSI}$ in the DCD group were significantly lower than those in the control group (Fig. 8(A), $P < 0.001$). The top, middle, and bottom W/D ratios in the DCD group were significantly higher than those in the control group (Fig. 8(B), $P < 0.001$). In addition, the top $SaO_{2\ MSI}$ and top W/D ratio were compared with those in middle and bottom $SaO_{2\ MSI}$. $\Delta SaO_{2\ MSI}$ of the top area, defined as top $SaO_{2\ MSI}$ – middle $SaO_{2\ MSI}$, was significantly lower than the $\Delta SaO_{2\ MSI}$ of the bottom area in both groups (control, $P = 0.038$; DCD, $P = 0.043$, Fig. 9(A)). In contrast, there was no difference between the top ΔW/D ratio and bottom ΔW/D ratio in the control group. The top ΔW/D ratio was significantly lower than the bottom ΔW/D ratio in the DCD group ($P = 0.003$, Fig. 9(B)).

3.5.   *SaO_2 error analysis*

Simulated SaO_2 in the lung are shown in Fig. 10(A). The error from the true value ($SaO_{2\ Perfusate}$ = $SaO_{2\ Lung}$ at k = 1) became larger as the value of k became smaller. $SaO_{2\ Lung}$ was underestimated

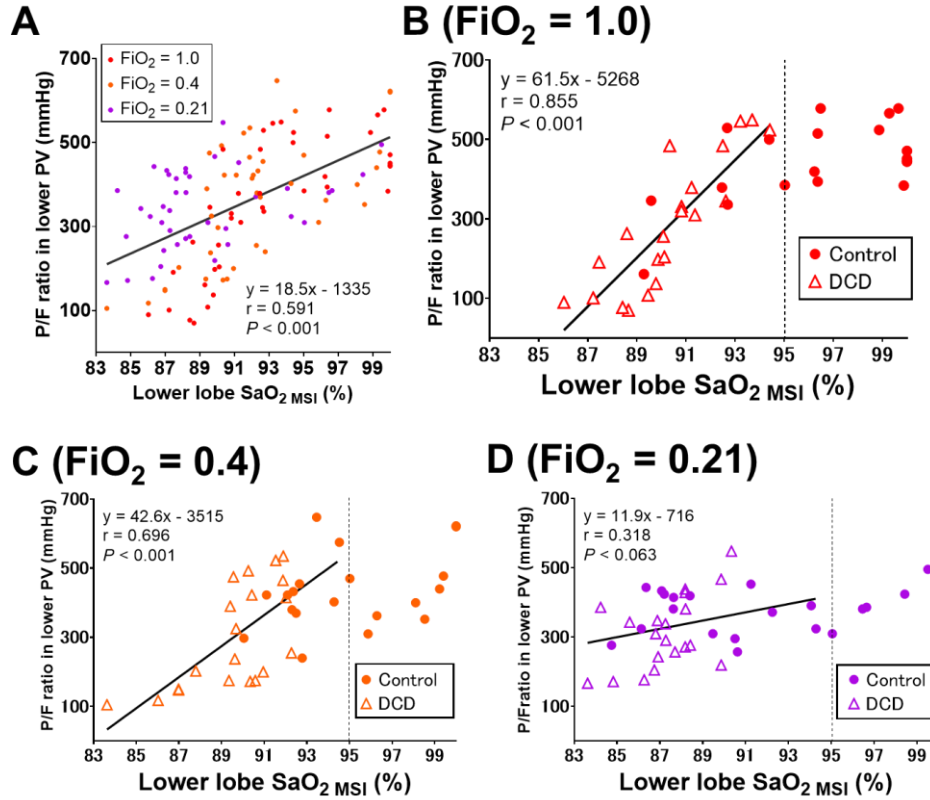**Fig. 7.** (A) Relationship between lower lobe $SaO_{2\ MSI}$ and P/F ratio in lower PV. There was a significant correlation between lower lobe $SaO_{2\ MSI}$ and P/F ratios in lower PV ($FiO_2 = 0.4$, 1.0, or 0.21; right and left side; 1 and 2 h; n = 120, r = 0.591, $P < 0.001$). (B) Relationship between lower lobe $SaO_{2\ MSI}$ and P/F ratios in lower PV at $FiO_2 = 1.0$ (n = 40, r = 0.855, $P < 0.001$). (C) Relationship between lower lobe $SaO_{2\ MSI}$ and P/F ratios in lower PV at $FiO_2 = 0.4$. n = 40 (r = 0.696, $P < 0.001$). (D) Relationship between lower lobe $SaO_{2\ MSI}$ and P/F ratios in lower PV at $FiO_2 = 0.21$. n = 40 (r = 0.318, $P = 0.063$).

as the $\mu'_{s\ Skeleton}$ became larger. The error disappeared as $SaO_{2\ Perfusate}$ became smaller. The mean error ΔSaO_2, defined as mean $SaO_{2\ Lung}$ - $SaO_{2\ Perfusate}$, is shown in Fig. 10(B). The mean error ΔSaO_2 was logarithmically reduced as k increased.
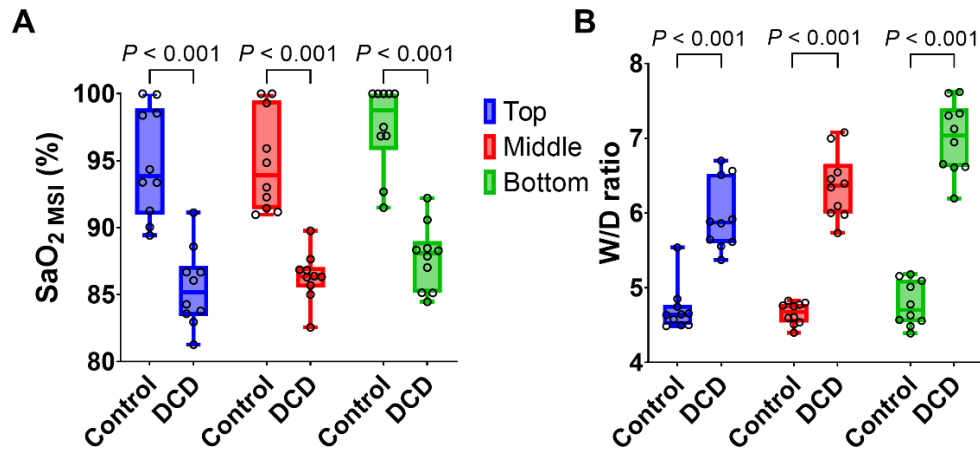
Fig. 8. (A) Comparison of top, middle, and bottom SaO_2 $_{MSI}$ between the control and DCD groups (Control, n = 10; DCD, n = 10, $P < 0.001$). (B) Comparison of top, middle, and bottom W/D ratios between the control and DCD groups (Control, n = 10; DCD, n = 10, $P < 0.001$).

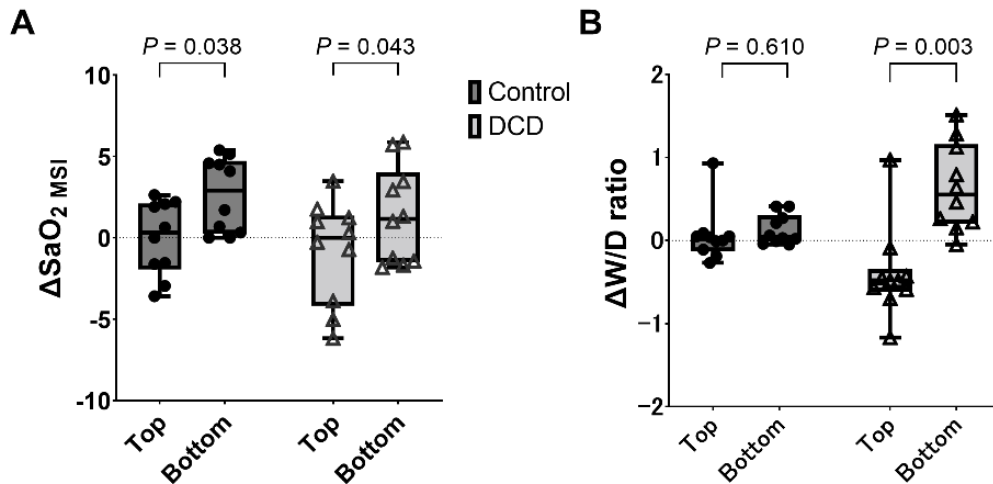**Fig. 9.** (A) ΔSaO_2 $_{MSI}$ of the top area (SaO_2 $_{MSI}$ in top area - SaO_2 $_{MSI}$ in middle area) was significantly lower than ΔSaO_2 $_{MSI}$ of the bottom area (SaO_2 $_{MSI}$ in bottom area - SaO_2 $_{MSI}$ in middle area) in both groups (Control, $P = 0.038$; DCD, $P = 0.043$). (B) There was no difference between the ΔW/D ratio of the top area (W/D ratio in top area - W/D ratio in middle area) and ΔW/D ratio of the bottom area (W/D ratio in bottom area - W/D ratio in middle area) in the control group. The ΔW/D ratio of the top area was significantly lower than the ΔW/D ratio of the bottom area in the DCD group ($P = 0.003$).
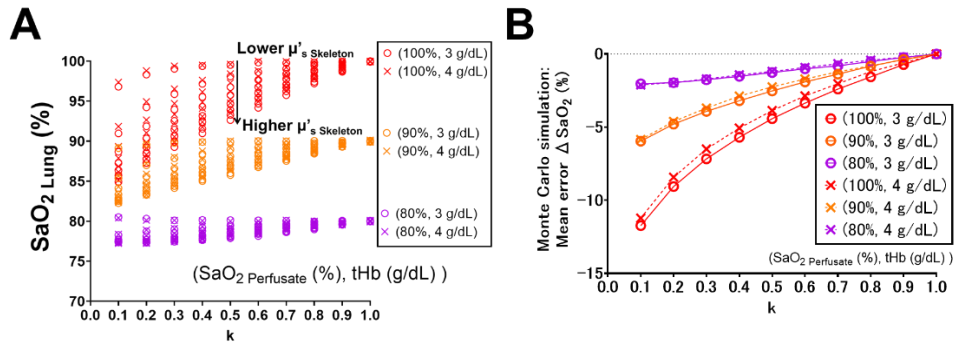
Fig. 10. (A) $SaO_{2\ Lung}$ shown in Eq. 8) distribution in each k value. ($\mu'_{s\ Skeleton}$ at 650 nm and $\mu'_{s\ Skeleton}$ at 800 nm) were altered from (2 cm^{-1}, 1 cm^{-1}) to (30 cm^{-1}, 27 cm^{-1}). (B) Mean error distribution: mean error ΔSaO_2 = mean $SaO_{2\ Lung}$ − $SaO_{2\ Perfusate}$.

4. Discussion

The most significant finding in this study was that reduced lower lobe $SaO_{2\ MSI}$ significantly correlated with low P/F ratios in lower PV and high W/D ratios of the lower lobes. This suggests that the proposed optical technique of SaO_2 imaging is a suitable for measuring extravascular lung water during cellular EVLP. Another important finding was that the correlation between lower lobe $SaO_{2\ MSI}$ and P/F ratio in the lower PV was the strongest at FiO_2 of 1.0 compared with FiO_2 of 0.4 and 0.21. This finding is consistent with our previous studies [17,26]. The P/F ratio at FiO_2 of 1.0 had the greatest area under the curve to detect non-suitable lungs. These findings are explained by the difference in the shunt fraction at each FiO_2.

In clinical EVLP, double lungs with a questionable single-side lesion are frequently perfused, and the EVLP team has to decide whether both lungs, a single lung, or neither are suitable for transplant. Our group demonstrated that the ultrasound monitoring of lung surface (CLUE) is useful for isolated lobe evaluation during clinical acellular EVLP [27]. However, SaO_2 imaging might be better to continuously monitor all of the lung surface area than ultrasound, because CLUE intermittently collects images from a limited number of locations. Therefore, the finding of an isolated single-side blue color spot or multiple and asymmetrical blue color spots in SaO_2 imaging could result in better detection of a single-side non-functioning lung. As there is no established method to diagnose pulmonary embolism during clinical EVLP, it may be a better fit for this technology.

In the relationship between lower lobe $SaO_{2\ MSI}$ and P/F ratio at FiO_2 of 1.0 (Fig. 7(B)), the P/F ratio reached a plateau at 500 mmHg, which corresponded to an $SaO_{2\ MSI}$ of 95%. This finding is different from that using a pulse oximeter for arterial oxygenation: there is a plateau of SaO_2 at 100%, because a pulse oximeter measures SaO_2 of arterial blood only. In contrast, $SaO_{2\ MSI}$ derives from a mixture of both venous and arterial blood. For example, brain SaO_2 using an optical tissue SaO_2 sensor, ForeSight Elite (Edwards Lifesciences Corp., CA, USA), shows a plateau of SaO_2 at 78% [28,29]. The mean ratio of venous/arterial mixture (*m*) for the brain has been determined to be 0.7 [28]. When SaO_2 in venous blood is 69% [29], the plateau point of brain tissue SaO_2 is calculated as follows: $m \times SaO_2$ in venous blood + (1-*m*) × SaO_2 in arterial blood = 0.7 × 69% + 0.3 × 100% = 78%. Similarly, MSI in our study captured backscattered light coming from both PA and PV. Hall et al. reported that the estimated ratio of the PA/PV mixture (*m*) in lungs is 0.5 [30]. Pure SaO_2 of PA was measured by using the perfusate sample from the outlet of the membrane oxygenator in our cases, and was 83%. When healthy lungs (the control group) are considered, the SaO_2 of pure PV will be 100%. Then, the plateau value

of SaO_2 $_{MSI}$ is estimated as $0.5 \times 83\% + 0.5 \times 100\% = 92\%$. The difference in the SaO_2 $_{MSI}$ plateau value between this estimation (92%) and our measured data (95%) might be explained by the potential variation in m of the lung superficial portion, where the MSI signal was collected, compared with whole lungs, including both superficial and deep portions. Another possibility is that SaO_2 $_{MSI}$ may be underestimated based on the results of the Monte Carlo simulations as discussed below. An additional important finding was that there was a significant difference in lower lobe SaO_2 $_{MSI}$ among the three areas: the top SaO_2 $_{MSI}$ in the lower lobes was significantly lower than those of the other areas. In addition, there was no difference in W/D ratios among the three areas in the control group, and anatomically, central and large-size PA was distributed in the top area, which might be because m is lower in the top area. These findings should be considered when interpreting SaO_2 imaging, especially when this technology is clinically applied. In this study, the dorsal side of the lower lobes was selectively evaluated by MSI technology. In early research by West et al., the '*gravitational model*' explains that the dorsal side of normal lungs has higher pulmonary blood pressure than the ventral side [31]. In addition, Niikawa et al. reported that there is a heterogeneous manifestation of ischemia reperfusion injury (IRI) during EVLP, with variations between upper and lower lobes [19]. In a supine position, the lower lobes have worse pulmonary function than the upper lobes. Based on these findings, a new setting of MSI monitoring the lower lobe selectively was developed in our study. When considering the significantly larger size of the lower lobe compared to upper lobe in pig lungs, selective SaO_2 monitoring of the lower lobes might be justified to detect signs of IRI.

In this study, the SaO_2 $_{MSI}$ was estimated by using the correlation between ΔR and the SaO_2 in perfusate samples from LA (Fig. 2). Ideally, the SaO_2 of perfusate inside the lungs should be compared with MSI images. However, in reality, it is impossible to collect perfusate samples from individual locations of lungs. Therefore, the degree of this discrepancy in SaO_2 was investigated by Monte Carlo simulations. The simulation results indicated that the error between SaO_2 $_{MSI}$ and true SaO_2 values in the lungs was limited as k (the volume ratio of perfusate/perfusate + skeleton) increased. In this study, as the first report of SaO_2 imaging of lung, we demonstrated the feasibility of the most basic two-wavelength SaO_2 imaging. The combination of two-wavelength band-pass filter and a digital camera can do the same imaging without using a hyperspectral camera. As a future prospective, three-wavelength oximetry using two isobestic wavebands [32,34], the theory of multispectral oximetry [33,34], and deep spectral learning approach [35] might provide more accurate SaO_2 $_{MSI}$ in EVLP. According to the gravitational model, ventilation/perfusion (V/Q) becomes less than 1 in the dependent area, suggesting that perfusate relatively increases with decreased alveolar size [31]. Therefore, it is expected that the k value in the dorsal side is high, suggesting that the data of SaO_2 $_{MSI}$ in this study included minimum discrepancy. This finding is consistent with the small difference in the SaO_2 $_{MSI}$ plateau value between the estimated SaO_2 (92%) and our measured data (95%).

This study has several limitations. First, porcine lungs were utilized with a limited case number. Further studies using human lungs are warranted. Second, the depth of backscattering light penetration was limited. According to a report by Stolik et al. [36], the estimated penetration depth in human lungs is in a range of 1-10 mm. Therefore, SaO_2 $_{MSI}$ data might reflect oxygenation in a relatively superficial portion of the lungs. However, based on the significant correlation between SaO_2 $_{MSI}$ and both P/F ratios in lower PV and W/D ratios, SaO_2 $_{MSI}$ might be a good surrogate for lower lobe pulmonary function. Third, the correspondence between SaO_2 image data and lung tissue for the W/D ratio can include a small gap.

5. Conclusion

A novel, noninvasive optical SaO_2 imaging system for cellular EVLP was developed using a porcine lung model. Lower lobe SaO_2 imaging significantly correlated with the P/F ratio in

lower PV. This technology provides noninvasive, continuous, and regional evaluation of lobular function in EVLP.

Disclosures. The authors declare no conflicts of interest.

Data availability. The datasets generated during and/or analyzed during the current study are available from the corresponding author on reasonable request.

References

1. S. Steen, R. Ingemansson, L. Eriksson, L. Pierre, L. Algotsson, P. Wierup, Q. Liao, A. Eyjolfsson, R. Gustafsson, and T. Sjöberg, "First human transplantation of a nonacceptable donor lung after reconditioning ex vivo," Ann. Thorac. Surg. **83**(6), 2191–2194 (2007).
2. A. Wallinder, S. E. Ricksten, C. Hansson, G. C. Riise, M. Silverborn, H. Liden, M. Olausson, and G. Dellgren, "Transplantation of initially rejected donor lungs after ex vivo lung perfusion," J. Thorac. Cardiovasc. Surg. **144**(5), 1222–1228 (2012).
3. P. Wierup, A. Haraldsson, F. Nilsson, L. Pierre, H. Scherstén, M. Silverborn, T. Sjöberg, U. Westfeldt, and S. Steen, "Ex vivo evaluation of nonacceptable donor lungs," The Annals of Thoracic Surgery **81**(2), 460–466 (2006).
4. J. Costa, S. Sreekanth, A. Kossar, K. Raza, D. J. Lederer, H. Robbins, L. Shah, J. R. Sonett, S. Arcasoy, and F. D'Ovidio, "Donor lung assessment using selective pulmonary vein gases," Eur J Cardiothorac Surg **50**(5), 826–831 (2016).
5. L. Freitag, D. Lenkens, P. Zarogoulidis, R. Karpf-Wisel, H. Hang, and K. Darwiche, "Functional bronchoscopy: development of a new bronchoscopic method for real-time gas exchange assessment of lobes and lung segments," Respiration **88**(6), 469–477 (2014).
6. R. M. Levenson and J. R. Mansfield, "Multispectral imaging in biology and medicine: slices of life," Cytometry **69A**(8), 748 (2006).
7. A. F. Goetz, G. Vane, J. E. Solomon, and B. N. Rock, "Imaging spectrometry for Earth remote sensing," Science **228**(4704), 1147 (1985).
8. G. Lu and B. Fei, "Medical hyperspectral imaging: a review," J. Biomed. Opt. **19**(1), 010901 (2014).
9. K. Bahram, J. M. Beach, and H. Kawano, "Hyperspectral imaging for measurement of oxygen saturation in the optic nerve head," Invest. Ophthalmol. Vis. Sci. 45(5), 1464–1472 (2004).
10. U. Rubins, Z. Marcinkevics, J. Cimurs, I. Saknite, E. Kviesis-Kipge, and A. Grabovskis, "Multimodal device for real-time monitoring of skin oxygen saturation and microcirculation function," Biosensors **9**(3), 97 (2019).
11. F. Tetschke, W. Markgraf, M. Gransow, S. Koch, C. Thiele, A. Kulcke, and H. Malberg, "Hyperspectral imaging for monitoring oxygen saturation levels during normothermic kidney perfusion," J. Sens. Sens. Syst. **5**(2), 313–318 (2016).
12. M. L. Polanyi and R. M. Hehir, "In vivo oximeter with fast dynamic response," Rev. Sci. Instrum. **33**(10), 1050–1054 (1962).
13. J. F. Beak, H. J. van Staveren, P. Posthumus, H. J. C. M. Sterenborg, and M. J. C. van Gemert, "The optical properties of lung as a function of respiration," Phy. Med. Biol. **42**(11), 2263 (1997).
14. J. Yi and V. Backman, "Imaging a full set of optical scattering properties of biological tissue by inverse spectroscopic optical coherence tomography," Opt. Lett. **37**(21), 4443–4445 (2012).
15. S. L. Jacques, "Optical properties of biological tissues: a review," Phys. Med. Biol. **58**(11), R37–R61 (2013).
16. M. K. Pasque, "Standardizing thoracic organ procurement for transplantation," J. Thorac. Cardiovasc. Surg. **139**(1), 13–17 (2010).
17. T. Okamoto, D. Wheeler, Q. Liu, C. Quintini, J. S. Hata, and K. R. McCurry, "Variability pressure of arterial oxygen to fractional inspired oxygen concentration ratio during cellular ex vivo lung perfusion: implication for decision making," Transplantation **99**(12), 2504–2513 (2015).
18. T. Okamoto, D. Wheeler, Q. Liu, C. Quintini, J. S. Hata, and K. R. McCurry, "Correlation between PaO_2/FiO_2 and airway and vascular parameters in the assessment of cellular ex vivo lung perfusion system," The Journal of Heart and Lung Transplantation **35**(11), 1330–1336 (2016).
19. H. Niikawa, T. Okamoto, K. S. Ayyat, Y. Itoda, C. F. Farver, and K. R. McCurry, "The protective effect of prone lung position on ischemia-reperfusion injury and lung function in an ex vivo porcine lung mode," J. Thorac. Cardiovasc. Surg. **157**(1), 425–433 (2019).

20. L. Wang, S. L. Jacques, and L. Zheng, "MCML—Monte Carlo modeling of light transport in multi-layered tissues," Computer Methods and Programs in Biomedicine **47**(2), 131–146 (1995).

21. G. Alexandrakis, F. R. Rannou, and A. F. Chatziioannou, "Tomographic bioluminescence imaging by use of a combined optical-PET (OPET) system: a computer simulation feasibility study," Phys. Med. Biol. **50**(17), 4225–4241 (2005).

22. D. Sakota and S. Takatani, "Photon-cell interactive Monte Carlo model based on the geometric optics theory for photon migration in blood by incorporating both extra- and intracellular pathways," J. Biomed. Opt. **15**(6), 065001 (2010).

23. W. Luo, S. Chen, D. Cheng, L. Wang, Y. Li, X. Ma, X. Song, X. Liu, W. Li, J. Liang, H. Yan, K. Zhao, C. Wang, L. Wang, and L. Zhang, "Genome-wide association study of porcine hematological parameters in a large white x minzhu F2 resource population," Int. J. Biol. Sci. **8**(6), 870–881 (2012).

24. P. W. Barber and S. C. Hill, *Light Scattering by Particles: Computational Methods* (World Scientific Pub. Co. Inc., 1990).

25. S. Prahl, "Optical absorption of hemoglobin," (1999) https://omlc.org/spectra/hemoglobin.

26. H. Niikawa, T. Okamoto, K. S. Ayyat, Y. Itoda, C. F. Farver, J. S. Hata, and K. R. McCurry, "A novel concept for evaluation of pulmonary function utilizing PaO_2/FiO_2 difference at the distinctive FiO_2 in cellular ex vivo lung perfusion—an experimental study," Transplant. Int. **32**(8), 797–807 (2019).

27. K. S. Ayyat, T. Okamoto, H. Niikawa, I. Sakanoue, S. Dugar, S. Q. Latifi, D. J. Lebovitz, A. Moghekar, and K. R. McCurry, "A CLUE for better assessment of donor lungs: Novel technique in clinical ex vivo lung perfusion," The Journal of Heart and Lung Transplantation **39**(11), 1220–1227 (2020).

28. C. C. Pang, "Measurement of body venous tone," J. Pharmacol. Toxicol. Methods **44**(2), 341–360 (2000).

29. K. Reinhardt, "Monitoring of mixed and central venous oxygen saturation in the critically III," *Practical Applications of Fiberoptics in Critical Care Monitoring*, F. R. Lewis, U. J. Pfeiffer, eds (Springer-Verlag Berlin Heidelberg, 1990), pp. 11–23.

30. J. E. Hall, "Pulmonary circulation, pulmonary edema, pleural fluid," *Guyton and Hall Textbook of Medical Physiology*, 13th ed. (Elsevier, 2015), p. 510.

31. J. B. West and C. T. Dollery, "Distribution of blood flow and ventilation-perfusion ratio in the lung, measured with radioactive carbon dioxide," J. Appl. Physiol. **15**(3), 405–410 (1960).

32. R. N. Pittman and B. R. Duling, "A new method for the measurement of percent oxyhemoglobin," J. Appl. Physiol. **38**(2), 315 (1975).

33. M. A. van der Putten, L. E. MacKenzie, A. L. Davies, J. Fernandez-Ramos, R. A. Desai, K. J. Smith, and A. R. Harvey, "A multispectral microscope for in vivo oximetry of rat dorsal spinal cord vasculature," Physiol. Meas. **38**(2), 205–218 (2017).

34. L. E. MacKenzie and A. Harvey, "Oximetry using multispectral imaging: theory and application," J. Opt. **20**(6), 063501 (2018).

35. R. Liu, S. Cheng, L. T. Tian, and J. Yi, "Deep spectral learning for label-free optical imaging oximetry with uncertainty quantification," Light. Sci. Appl. **8**(1), 102 (2019).

36. S. Stolik, J. A. Delgado, A. Perez, and L. Anasagasti, "Measurement of the penetration depths of red and near infrared light in human "ex vivo" tissues," J. Photochem. Photobiol. B. **57**(2-3), 90–93 (2000).